Metallothionein 1G promotes the differentiation of HT-29 human colorectal cancer cells

JUAN MARTÍN ARRIAGA[1,2], ALICIA INÉS BRAVO[3], JOSÉ MORDOH[1,2,4] and MICHELE BIANCHINI[2]

[1]Cancerology Laboratory, Leloir Institute, IIBBA-CONICET, Buenos Aires 1405;
[2]Center for Oncology Research, Cancer Foundation (CIO-FUCA), Buenos Aires 1426;
[3]Acute Interzonal General Hospiutal 'Eva Perón', Buenos Aires 1650;
[4]Alexander Fleming Institute, Buenos Aires 1180, Argentina

Received September 27, 2016; Accepted November 16, 2016

DOI: 10.3892/or.2017.5547

Abstract. Metallothioneins (MTs) are a family of low-molecular-weight, cysteine-rich proteins involved in zinc and redox metabolism, that are epigenetically downregulated during colorectal cancer (CRC) progression, but may be re-induced with a variety of agents. Since loss of MT expression is associated with a worse prognosis, in the present study we investigated the effects of overexpression of the most significantly downregulated isoform in CRC, namely MT1G, on the HT-29 cell line. Overexpression of MT1G resulted in xenograft tumors with an aberrant morphology, characterized by an evident increase in mucin-containing cells that were identified as goblet cells under electron microscopy. Immunohistochemical detection of CDX2 and cytokeratin 20 was also increased, as were goblet-cell and enterocyte-specific genes by qRT-PCR. Microarray analysis of gene expression confirmed the alteration of several differentiation signaling pathways, including the Notch pathway. Using sodium butyrate and post-confluent growth as inducers of differentiation, we demonstrated that MT1G does indeed play a functional role in promoting goblet over enterocyte differentiation *in vitro*. Labile zinc is also induced upon differentiation of CRC cells, functionally contributing to enterocyte over goblet differentiation, as revealed using zinc-specific chelating agents. Overall, our results uncover a new tumor-suppressor activity of MT1G in promoting the differentiation of at least some CRC tumors, and implicate MTs and zinc signaling as new players in colorectal differentiation. This further contributes to the hypothesis that re-induction of MTs may have therapeutic value by diminishing the aggressiveness of CRC tumors.

Correspondence to: Dr Juan Martín Arriaga, Cancerology Laboratory, Leloir Institute, IIBBA-CONICET, Avenida Patricias Argentinas 435, Buenos Aires 1405, Argentina
E-mail: jm_arriaga@yahoo.com.ar

Abbreviations: BUT, sodium butyrate; CRC, colorectal cancer; FZ, fluozin 3-AM; MMPs, matrix metalloproteinases; TPEN, N,N,N',N'-tetrakis(2-pyridylmethyl) ethylenediamine; MTs, metallothioneins

Key words: metallothioneins, labile zinc, colorectal cancer, goblet cells, differentiation

Introduction

Colorectal cancer (CRC) is the third most commonly diagnosed cancer worldwide, having a mortality rate near 50% (1). Recent studies have shown that these tumors retain multilineage differentiation processes similar to those of the normal intestinal epithelium, mainly the goblet cell and enterocyte lineages (2). Furthermore, molecular classifications representing these cellular phenotypes can have prognostic value and be predictive of response to different therapeutic agents (3).

Metallothioneins (MTs) are a family of low-molecular-weight, cysteine-rich proteins involved in zinc and redox metabolism. By chelating zinc ions through redox-active thiol groups, they have the capacity to regulate the exchangeable, loosely-bound pool of intracellular zinc, termed the 'labile' pool, which participates in zinc transfer reactions and intracellular signaling. Thus MTs have been implicated in many aspects of tumor biology, such as proliferation, differentiation, apoptosis, angiogenesis, redox and zinc homeostasis, anti-inflammatory reactions and immunomodulation (4-7). The human genome encodes at least 11 functional MT isoforms that share structural and functional similarities. Due to their structural similarity, commercially available antibodies do not distinguish between individual MT isoforms, and therefore their individual mRNA expression levels can be measured by qRT-PCR. However, due to the fact that they are variably expressed in tissues and induced by several stimuli, it is possible that different tumors express distinct MT genes, which could help explain the conflicting data on MT function in different tumor types (6,7). We and others have previously shown that multiple MT1 isoforms and MT2A are downregulated during CRC progression (especially isoform MT1G) mainly through epigenetic mechanisms, and that this is associated with shorter patient survival (8-11). Several agents such as DNA methyltransferase inhibitors, histone deacetylase inhibitors or zinc are capable of re-inducing MT expression in colorectal tumors, which can

slow down *in vivo* tumor growth and sensitize these tumors to chemotherapeutic agents (12).

In order to help understand the phenotypic consequences of MT induction, in the present study we investigated the effects of stable overexpression of the most downregulated isoform in CRC, namely MT1G, on the HT-29 CRC cell line. We uncovered a new role for this isoform in modulating tumor differentiation and thus expand the mechanisms by which this gene may act as a tumor suppressor in CRC.

Materials and methods

Reagents and cell lines. The MT1G cDNA was cloned into the pcDNA3.1/myc-His(-)A expression vector, resulting in an MT1G-myc fusion protein as previously described (12). Sodium butyrate and N,N,N',N'-tetrakis(2-pyridylmethyl) ethylenediamine (TPEN) were purchased from Sigma-Aldrich Inc. (St. Louis, MO, USA), and FluoZin-3-AM (FZ) from Invitrogen (San Diego, CA, USA). The human CRC cell lines HT-29 and HCT116 were obtained from the American Type Culture Collection (ATCC; Manassas, VA, USA), maintained as previously described (8), and subjected to STR profiling for authentication after all experiments were finalized. For post-confluent growth, day 0 was considered the day when cells reached 100% confluence, and fresh medium was replaced every 1-2 days thereafter.

Animal studies and histological procedures. Eight- to 10-week-old male nude mice were subcutaneously injected ($2x10^6$ cells each) with two independent clones of MOCK or $MT1G^+$ cells (5 mice/group) and tumor size was measured with a caliper to calculate tumor volume using the formula: Tumor volume (mm^3) = [length (mm)] x [width (mm)]^2 x $\pi/6$. All animal procedures were approved by the Institutional Animal Care Board of the Leloir Institute. After 50 days, tumors were excised, formalin-fixed and paraffin-embedded for histological examination. A fraction of each tumor was preserved in RNAlater medium (Ambion Inc., Austin TX, USA) at 4˚C for 24 h, and then stored at -80˚C. RNA was extracted from RNAlater-preserved tissues using the TRIzol method (Invitrogen), and quantification and quality control were performed with the Agilent 2100 Bioanalyzer (Agilent Technologies, Santa Clara, CA, USA). Paraffin sections (4 μm thick) were re-hydrated and stained with Alcian Blue stain (1% in 3% acetic acid, pH 2.5) or processed for immunohistochemistry using the Vectastain Universal Elite ABC kit (Vector Laboratories, Inc., Burlingame, CA, USA) with citrate buffer antigen retrieval and the following antibodies: anti-cytokeratin 20 (KS 20.8; Dako Corporation, Carpinteria, CA, USA) and anti-CDX2 (clone EPR2764Y; Cell Marque, Rocklin, CA, USA).

For transmission electron microscopy, freshly xenografted tumors were cut into small (~1-mm thick) pieces and promptly fixed in 2.5% glutaraldehyde in phosphate-buffered saline (PBS) for 2 h, washed and fixed for 90 min in 1% osmium tetroxide in phosphate-buffered saline (PBS), de-hydrated in acetone gradients and included in resin. Semi-(0.5 μm) and ultra-thin (70 nm) sections were cut and contrasted in 2.5% uranyl-acetate, and visualized using a Zeiss EM 109T microscope coupled to a digital CCD Gatan ES1000W camera.

Gene expression profile analysis and qRT-PCR. Total RNA was extracted, and mRNA expression was analyzed using an Agilent Custom microarray 8x15K (Agilent Technologies, Palo Alto, CA, USA), which contained 15,744 oligonucleotide probes representing >8,200 different human transcripts. Two samples from each group were used to detect mRNA expression; each biological replicate was run in duplicate, and the fluorochromes were swapped to reduce dye-bias; in total eight 15K microarrays were scanned using the Axon Confocal Scanner 4000B (Molecular Devices, Sunnyvale, CA, USA) with optimized settings: dye channel, 635 nm, PMT=720, laser power, 30%, scan resolution, 10 nm; dye channel, 532 nm, PMT=540, laser power, 30%, scan resolution, 10 nm; line average, 4 lines. The data were analyzed using GenePix® Pro 6 Microarray Acquisition and Analysis Software (Molecular Devices) and normalized with the MIDAS v2.2: Microarray Data Analysis System (TIGR's Microarray Data Analysis System). Normalization was necessary to compensate for variability between slides and fluorescent dyes. To this end we employed a locally weighted linear regression [Lowess (13,14)]; data were filtered using low-intensity cutoff and replicate consistency trimming.

The differentially expressed genes among the $MT1G^+$, and control (MOCK) sets were identified using the significant analysis of microarray (SAM) statistical software from MultiExperiment Viewer (MeV) (TIGR's Microarray Data Analysis System). In the comparisons of $MT1G^+$ vs. MOCK, the genes that were all upregulated in the comparisons were identified as the persistently upregulated genes, and the genes that were all downregulated in the comparisons were defined as the persistently downregulated genes.

The gene annotation enrichment analysis using Gene Ontology (GO) (http://www.geneontology.org/) and Kyoto Encyclopedia of Genes and Genomes (KEGG) (http://www.genome.jp/kegg/) data for gene sets was performed using Database for Annotation, Visualization, and Integrated Discovery (DAVID) software (15,16). A Benjamini p-value of 0.05 was used in the analysis.

Quantitative reverse-transcription PCR (qRT-PCR) was used to quantify mRNA levels as previously described (8). Briefly, PCR runs were carried out using SYBR Universal Master Mix (Applied Biosystems, Carlsbad, CA, USA), and relative expression levels were determined by the $\Delta\Delta$Ct method using ACTB gene expression to normalize all samples. The primers used are listed in Table I.

Alkaline phosphatase activity measurement. The activity of this enzyme was used as a marker of differentiation of HT-29 cells (17). For this purpose, confluent cell lines were lysed in 10 mM Tris (pH 7.4), 1 mM $MgCl_2$, 20 μM $ZnCl_2$, 0.2% Triton X-100 + protease inhibitors, and incubated with NBT-BCIP as the chromogenic substrate for 16 h at 37˚C. The resulting brown precipitate was solubilized in 10% SDS, 10% HCl and absorbance was measured at 595 nm.

siRNA transfection. Two siRNAs targeting the MT1G isoform (si1G.1 and si1G.2) and one targeting all functional MT-1 and MT-2 isoforms were previously validated (12), and transfected at 125 nM using LF2000 (Invitrogen) as described by the manufacturer. After 24 h of siRNA treatment, medium was replaced

Table I. Primer sequences.

Gene	Forward primer	Reverse primer
MT1G	CTTCTCGCTTGGGAACTCTA	AGGGGTCAAGATTGTAGCAAA
MT2A	GCAACCTGTCCCGACTCTAG	TTGCAGGAGGTGCATTTG
ACTB	GCCATCTCTTGCTCGAAGTCCAG	ATGTTTGAGACCTTCAACACCCC
CDKN1A	AAGACCATGTGGACCTGT	GGTAGAAATCTGTCATGCTG
HSI	GAGGACACTGGCTTGGAGAC	ATCCAGCGGGTACAGAGATG
HALPI	GACCACTCCCATGTCTTCTCCTT	TCGCACGCCTGAGTTGAA
CA2	CCGCGGACACACAGTGCAGG	CCAGTGCTCAGGTCCGTTGTGT
CA1	CAGAACATACAGTGGATGGAGTCAA	GGCCTCACCAACCTTCATCA
K20	AAATGCTCGGTGTGTCCTG	ACTTCCTCCTGATGCTCCTT
ATOH1	CCCCGGGAGCATCTTG	GGGACCGAGGCGAAGTT
TFF3	CTCCAGCTCTGCTGAGGAGT	GCTTGAAACACCAAGGCACT
HMUC2	CAGCACCGATTGCTGAGTTG	GCTGGTCATCTCAATGGCAG
CDX2	GATGGTGATGTAGCGACTGTAGTGA	CTCGGCAGCCAAGTGAAAAC

with or without 2 mM sodium butyrate for 48 h, and cells were collected for RNA extraction or ALP activity measurement.

Scratch assays and gelatin zymography. We used the scratch assay to estimate the migration capacities of MOCK and MT1G$^+$ cell lines, which were plated in triplicate in 24-well plates until they reached confluence. Two perpendicular scratches were made with a pipette tip, after which the cells were washed thrice in PBS and replaced with 1% fetal bovine serum (FBS) medium. Areas with the same wound length were selected and photographed until complete wound closure. Wound closure at a given time t was calculated as: (initial wound length - wound length at time t)/initial wound length x 100.

To determine gelatinase activity of matrix metalloproteinases (MMPs), upon reaching confluence medium was replaced with serum-free Dulbecco's modified Eagle's medium (DMEM) for 24 h, and the conditioned medium was centrifuged at 1,200 x g for 5 min, and immediately loaded into 10% polyacrylamide electrophoretic gels with or without 2.5 mg/ml gelatin (Sigma-Aldrich) as described in (18). Coomasie Blue staining of the non-gelatin gels were used as a loading control.

Measurement of intracellular labile zinc. For this purpose we employed the cell-permeable zinc-specific fluorophore FZ as described in (12). Briefly, cells were plated in triplicate in sterile plastic coverslips (for fluorescence microscopy) or in 96-well plates (for fluorimetric analysis), and incubated for 30 min at room temperature with 2 μM FZ in PBS, washed in PBS and incubated a further 30 min in PBS at room temperature. Propidium iodide staining was used to control for plating differences and data are expressed as normalized fluorescence FZ = (F - FTPEN)/(FZn - FTPEN), so as to get values relative to a 'maximum' intensity given by pretreatment with zinc 400 μM for 8 h (FZn, resulting in FZ=1) and a 'minimum' intensity given by 20 μM TPEN treatment during the final 30 min incubation of fluozin (FTPEN, resulting in FZ=0). This score allowed us to better compare results of the different experiments.

Statistical analysis. Data are expressed as mean ± SEM and p-values <0.05 were considered significant. Comparison of means was carried out using Student's t-test, with one-way ANOVA followed by Dunnett's post hoc t-test for three or more groups, or with two-way ANOVA followed by Bonferroni's post hoc t-test for two variables. GraphPad Prism 5.0 (GraphPad Software, Inc., La Jolla, CA, USA) software was used for analysis.

Results

MT1G overexpression in the HT-29 CRC cell line. We stably expressed MT1G as a myc-epitope fusion protein in HT-29 cells. When grown *in vivo* as subcutaneous xenografts on nude mice, these MT1G$^+$ cells grew at similar rates compared to the empty-vector ('MOCK')-transfected cells (data not shown), in stark contrast to the antiproliferative effects we had previously observed using the HCT116 cell line (12). However, hematoxylin and eosin (H&E) staining (Fig. 1A) showed that MT1G$^+$ tumors contained a higher number of mucin-containing, Alcian Blue-positive cells (Fig. 1B) that were confirmed to be goblet cells by transmission electron microscopy (Fig. 1C). Nuclear expression of the intestine-specific homeobox transcription factor CDX2 was markedly enhanced in the MT1G$^+$ tumors, as shown by immunohistochemical staining on Fig. 1D, as was also the intensity of cytokeratin 20 (Fig. 1E). The latter also suggests that commitment to the enterocyte lineage may be enhanced as well. Indeed, both goblet-associated (*TFF3*, *ATOH1* and *MUC2*) and enterocyte-associated genes (*HSI*, *CA2* and *ALPI*) were overexpressed in the MT1G$^+$ tumors by qRT-PCR analysis (Fig. 1F), suggesting that MT1G$^+$ tumors are more differentiated than MOCK controls.

Gene expression analysis of HT-29 MT1G$^+$ tumors using cDNA microarrays. We then used cDNA microarrays to profile the mRNA expression of MOCK and MT1G$^+$ HT-29 xenografts, derived from two different MT1G$^+$ or MOCK clonal cell lines (MT1G-1 and MT1G-2, or MOCK-1 and

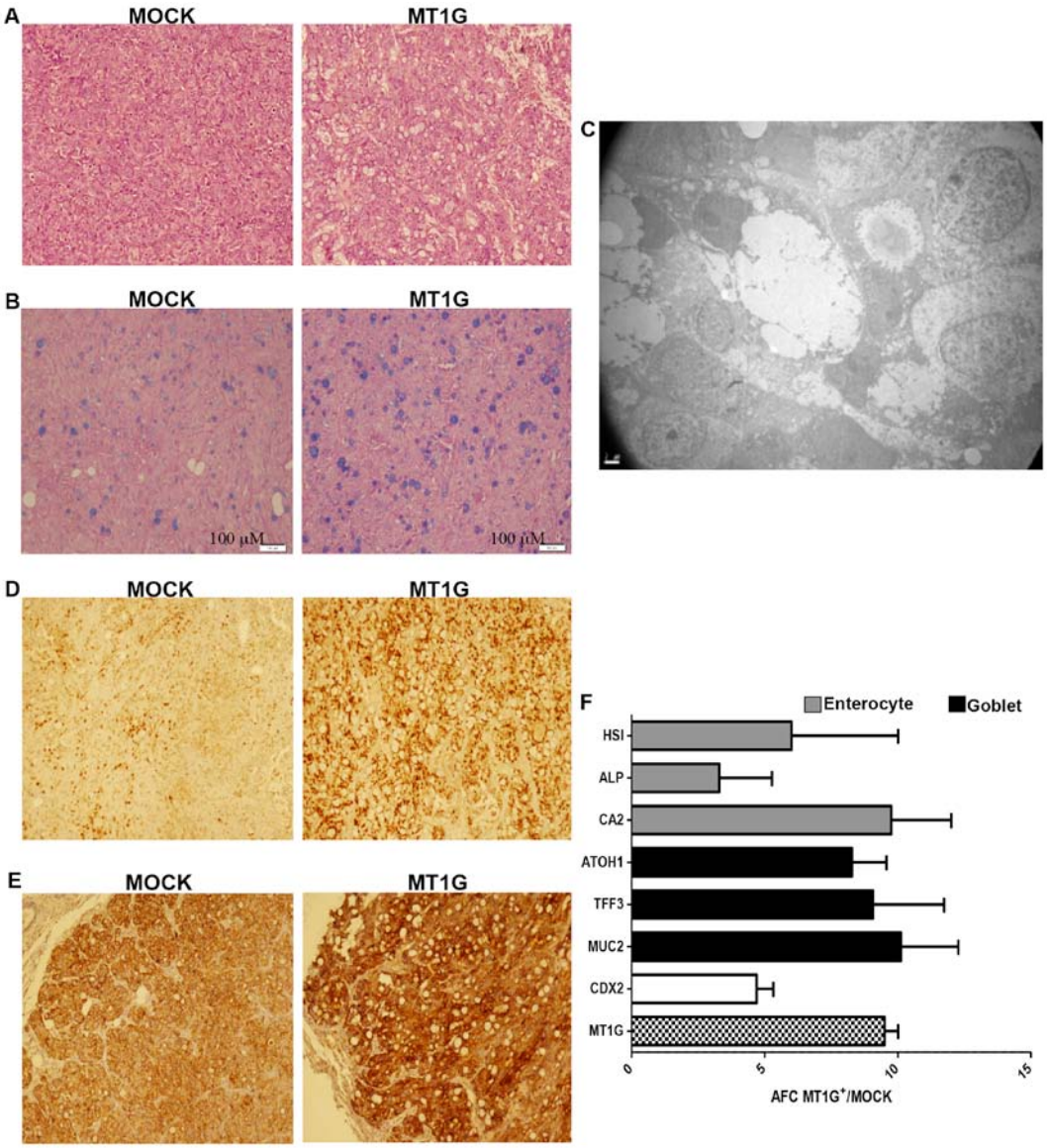

Figure 1. HT-29 MOCK and MT1G$^+$ subcutaneous xenografts in nude mice. (A) H&E and (B) Alcian Blue stainings showing an increase in the number of mucin-like cells in the MT1G$^+$ tumors. (C) Microphotograph of a goblet-like cell in MT1G$^+$ tumors. (D) CDX2 and (E) keratin 20 immunohistochemistry. (F) Expression of enterocyte and goblet-associated differentiation markers, as assessed by qRT-PCR. AFC, average fold-change.

MOCK-2, respectively). Gene expression profiles of the biological replicates were reproducible and highly correlated (Pearson's correlation coefficient 0.81). Analysis of data with Rank product analysis revealed significant gene expression differences among the groups, with a total of 305 known genes found to be consistently upregulated or downregulated in the MT1G$^+$ tumors (Table II). GO analysis indicated that several functional categories were enriched by DAVID, and included upregulated genes associated with cell differentiation, cell fate commitment and Notch signaling pathway, as well as down-regulated genes in the categories of regulation of apoptosis, cell migration and cell proliferation (Table III). Differentially expressed genes were also analyzed for KEGG pathway enrichment and two significantly enriched pathways were identified between upegulated or downregulated genes: the Notch signaling pathway and pathways in cancer, respectively.

Given the finding of downregulated genes in the cell migration category, we performed migration 'scratch' assays in the HT-29 and HCT116 cell lines overexpressing MT1G, and found in both cell lines a statistically significant reduction in migration rates upon MT1G overexpression (Fig. 2A and B). Gelatin zymography using conditioned media from these cells, however, revealed no differences in MMP2 activity (Fig. 2C).

Next, in order to further investigate the involvement of MT1G in the differentiation of HT-29 cells, we used two different and well-known cell culture conditions to stimulate the *in vitro* differentiation of these cells: sodium butyrate (BUT) treatment (19) and post-confluent cell growth (20). We used *TFF3* and *MUC2* mRNA expression as surrogate markers for the goblet cell lineage, and *HSI* and *CA1* mRNAs, along with enzymatic alkaline-phosphatase activity (ALP) for enterocytes.

Involvement of MT1G in butyrate-mediated differentiation of HT-29 cells. Sodium butyrate is a well-known inducer of differentiation in CRC cell lines (21), and indeed, as shown in

Table II. List of all significantly differentially expressed genes in MT1G+ vs. MOCK HT-29 xenografts.

A, Upregulated genes

Gene reference	Gene symbol	Name	Mean	P-values (Up)	RP-values (Up)
NM_138444	KCTD12	Potassium channel tetramerisation domain containing 12	2.65	2.81E-06	80.00
NM_000051	ATM	Ataxia telangiectasia mutated	2.52	4.68E-06	91.77
NM_175698	SSX2	Synovial sarcoma, X breakpoint 2	3.06	6.56E-06	99.19
NM_031964	KRTAP17-1	Keratin-associated protein 17-1	2.35	2.25E-05	141.15
NM_003357	SCGB1A1	Secretoglobin, family 1A, member 1 (uteroglobin)	2.19	2.72E-05	155.94
NM_005430	WNT1	Wingless-type MMTV integration site family, member 1	2.40	2.81E-05	156.29
NM_001031672	CYB5RL	Cytochrome b5 reductase-like	2.37	3.18E-05	164.29
NM_000546	TP53	Tumor protein p53	2.12	3.75E-05	168.99
NM_001123065		Chromosome 7 open reading frame 65	2.04	4.59E-05	181.40
NM_001443	FABP1	Fatty acid binding protein 1, liver	2.27	5.99E-05	197.89
NM_000364	TNNT2	Troponin T type 2 (cardiac)	2.01	8.24E-05	216.07
NM_001201	BMP3	Bone morphogenetic protein 3	2.17	1.01E-04	224.84
NM_031310	PLVAP	Plasmalemma vesicle-associated protein	2.02	1.22E-04	239.78
NM_182981	OSGIN1	Oxidative stress induced growth inhibitor 1	1.89	1.44E-04	249.22
NM_139211	HOPX	HOP homeobox	1.88	1.65E-04	256.18
NM_017774	CDKAL1	CDK5 regulatory subunit-associated protein 1-like 1	1.86	2.00E-04	271.00
NM_001077195	ZNF436	Zinc finger protein 436	1.96	2.62E-04	289.52
NM_000067	CA2	Carbonic anhydrase II	1.76	2.82E-04	295.37
NM_015894	STMN3	Stathmin-like 3	1.17	2.86E-04	296.25
NM_014237	ADAM18	ADAM metallopeptidase domain 18	2.19	2.95E-04	298.48
NM_182705	FAM101B	Family with sequence similarity 101, member B	1.81	4.28E-04	330.71
NM_025191	EDEM3	ER degradation enhancer, α-mannosidase-like 3	1.78	4.56E-04	337.06
NM_020639	RIPK4	Receptor-interacting serine-threonine kinase 4	1.70	4.56E-04	337.43
NM_004557	NOTCH4	Notch 4	1.70	4.77E-04	340.80
NM_005618	DLL1	δ-like 1 (*Drosophila*)	1.70	5.05E-04	346.21
NM_004001	FCGR2B	Fc fragment of IgG, low affinity IIb, receptor (CD32)	1.71	5.22E-04	349.94
NM_001008225	CNOT4	CCR4-NOT transcription complex, subunit 4	1.66	6.17E-04	367.80
NM_170664	OTOA	Otoancorin	1.64	6.23E-04	368.88
NM_019845	RPRM	Reprimo, TP53-dependent G2 arrest mediator candidate	1.39	6.24E-04	369.37
NM_033409	SLC52A3	Chromosome 20 open reading frame 54	1.65	6.26E-04	369.79
NM_001010879	ZIK1	Zinc finger protein interacting with K protein 1 homolog (mouse)	1.59	6.68E-04	376.61
NM_007365	PADI2	Peptidyl arginine deiminase, type II	1.98	6.99E-04	381.36
NM_007314	ABL2	v-abl Abelson murine leukemia viral oncogene homolog 2	0.99	7.21E-04	385.01
NM_001080519	BAHCC1	BAH domain and coiled-coil containing 1	1.58	7.93E-04	397.25
NM_000584	CXCL8	Interleukin 8	1.68	9.46E-04	419.56
NM_002649	PIK3CG	Phosphoinositide-3-kinase, catalytic, γ-polypeptide	1.74	1.07E-03	437.34
NM_178311	GGTLC1	γ-glutamyltransferase light chain 1	1.28	1.09E-03	440.27
NM_001124756	PABPC1L	Poly(A) binding protein, cytoplasmic 1-like	1.51	1.11E-03	442.81
NM_001010926	HES5	Hairy and enhancer of split 5 (*Drosophila*)	1.09	1.15E-03	446.74
NM_152643	KNDC1	Kinase non-catalytic C-lobe domain (KIND) containing 1	1.85	1.18E-03	449.71

Table II. Continued.

Gene reference	Gene symbol	Name	Mean	P-values (Up)	RP-values (Up)
NM_152279	ZNF585B	Zinc finger protein 585B	1.30	1.18E-03	450.06
NM_003018	SFTPC	Surfactant protein C	1.51	1.20E-03	452.03
NM_003460	ZP2	Zona pellucida glycoprotein 2 (sperm receptor)	1.79	1.23E-03	456.86
NM_022101		Chromosome X open reading frame 56	0.84	1.30E-03	464.79
NM_001136566	RAD21L1	RAD21-like 1 (*S. pombe*)	0.61	1.31E-03	465.53
NM_019886	CHST7	Carbohydrate (N-acetylglucosamine 6-O) sulfotransferase 7	1.49	1.43E-03	477.78
NM_002410	MGAT5	Mannosyl (α-1,6-)-glycoprotein β-1,6-N-acetyl-glucosaminyltransferase	1.37	1.49E-03	484.02
NM_001130715	PLAC8	Placenta-specific 8	1.47	1.51E-03	485.05
NM_012368	OR2C1	Olfactory receptor, family 2, subfamily C, member 1	1.42	1.60E-03	493.64
NM_198463	C3ORF67	Chromosome 3 open reading frame 67	1.55	1.72E-03	503.50
NM_080647	TBX1	T-box 1	1.01	1.74E-03	504.66
NM_001136003	C2CD4D	C2 calcium-dependent domain containing 4D	1.38	1.83E-03	512.27
NM_014909	VASH1	Vasohibin 1	1.38	1.84E-03	512.54
NM_002318	LOXL2	Lysyl oxidase-like 2	1.44	1.91E-03	518.96
NM_031457	MS4A8	Membrane-spanning 4-domains, subfamily A, member 8B	1.36	2.17E-03	538.29
NM_001146190	ZNF407	Zinc finger protein 407	1.35	2.20E-03	541.10
NM_004375	COX11	COX11 cytochrome *c* oxidase assembly homolog (yeast)	1.37	2.36E-03	552.91
NM_001040462	BTNL8	Butyrophilin-like 8	0.84	2.39E-03	554.54
NM_001265	CDX2	Caudal type homeobox 2	1.33	2.44E-03	558.57
NM_001013661	VSIG8	V-set and immunoglobulin domain containing 8	1.33	2.50E-03	563.31
NM_019119	PCDHB9	Protocadherin-β9	1.32	2.51E-03	564.49
NM_001144875	DOK3	Docking protein 3	1.29	2.54E-03	566.33
NM_003722	TP63	Tumor protein p63	1.38	2.56E-03	569.10
NM_006138	MS4A3	Membrane-spanning 4-domains, subfamily A, member 3 (hematopoietic cell-specific)	1.58	2.73E-03	580.41
NM_005427	TP73	Tumor protein p73	1.37	2.88E-03	589.30
NM_003106	SOX2	SRY (sex determining region Y)-box 2	1.07	3.12E-03	604.10
NM_033318	SMDT1	Chromosome 22 open reading frame 32	0.80	3.14E-03	605.59
NM_012426	SF3B3	Splicing factor 3b, subunit 3, 130 kDa	1.31	3.31E-03	615.60
NM_002458	MUC5B	Mucin 5B, oligomeric mucus/gel-forming	1.53	3.45E-03	623.75
NM_001001411	ZNF676	Zinc finger protein 676	1.45	3.48E-03	625.90
NM_000362	TIMP3	TIMP metallopeptidase inhibitor 3	1.33	3.55E-03	629.94
NM_014751	MTSS1	Metastasis suppressor 1	1.23	3.62E-03	633.32
NM_201442	C1S	Complement component 1, s subcomponent	0.91	3.63E-03	633.68
NM_005961	MUC6	Mucin 6, oligomeric mucus/gel-forming	1.21	3.92E-03	647.05
NM_001002758	PRY2	PTPN13-like, Y-linked 2	1.47	3.99E-03	650.48
NM_001135654	PABPC4	Poly(A) binding protein, cytoplasmic 4 (inducible form)	1.31	4.01E-03	651.26
NM_014030	GIT1	G protein-coupled receptor kinase interacting ArfGAP 1	1.17	4.13E-03	657.53
NM_001083537	FAM86B1	Family with sequence similarity 86, member B1	1.29	4.16E-03	658.91
NM_001645	APOC1	Apolipoprotein C-I	1.20	4.27E-03	664.10
NM_003226	TFF3	Trefoil factor 3 (intestinal)	1.19	4.29E-03	664.92
NM_005172	ATOH1	Atonal homolog 1 (*Drosophila*)	1.26	4.31E-03	665.93

Table II. Continued.

Gene reference	Gene symbol	Name	Mean	P-values (Up)	RP-values (Up)
NM_003708	RDH16	Retinol dehydrogenase 16 (all-*trans*)	0.92	4.41E-03	670.22
NM_002917	RFNG	RFNG O-fucosylpeptide 3-β-N-acetylglucosaminyltransferase	1.28	4.56E-03	677.43
NM_016585	THEG	Theg homolog (mouse)	1.19	4.63E-03	681.11
NM_007058	CAPN11	Calpain 11	1.51	4.73E-03	684.84
NM_003759	SLC4A4	Solute carrier family 4, sodium bicarbonate co-transporter, member 4	1.19	4.74E-03	685.17
NM_020299	AKR1B10	Aldo-keto reductase family 1, member B10 (aldose reductase)	1.17	4.77E-03	686.57
NM_032133	MYCBPAP	MYCBP-associated protein	0.92	4.95E-03	693.39
NM_001631	ALPI	Alkaline phosphatase, intestinal	1.25	4.98E-03	695.09
NM_002486	NCBP1	Nuclear cap binding protein subunit 1, 80 kDa	1.23	5.09E-03	699.73
NM_001105659	LRRIQ3	Leucine-rich repeats and IQ motif containing 3	1.18	5.13E-03	702.05
NM_014276	RBPJL	Recombination signal binding protein for immunoglobulin-κJ region-like	1.15	5.29E-03	708.75
NM_015461	ZNF521	Zinc finger protein 521	0.91	5.35E-03	711.10
NM_001105662		Ubiquitin specific peptidase 17	1.21	5.63E-03	722.91
NM_005068	SIM1	Single-minded homolog 1 (*Drosophila*)	1.19	5.73E-03	726.21
NM_018646	TRPV6	Transient receptor potential cation channel, subfamily V, member 6	0.64	6.05E-03	739.17
NM_139026	ADAMTS13	ADAM metallopeptidase with thrombospondin type 1 motif, 13	0.84	6.31E-03	749.50
NM_152749	ATXN7L1	Ataxin 7-like 1	0.75	6.31E-03	749.64
NM_019034	RHOF	Ras homolog gene family, member F (in filopodia)	1.21	6.35E-03	751.22
NM_017592	MED29	Mediator complex subunit 29	0.92	6.38E-03	752.10
NM_206965	FTCD	Formiminotransferase cyclodeaminase	1.16	6.40E-03	752.88
NM_020063	BARHL2	BarH-like homeobox 2	1.10	6.41E-03	753.43
NM_016338	IPO11	Importin 11	0.74	6.51E-03	756.92
NM_001109997	KLHL33	Kelch-like 33 (*Drosophila*)	1.15	6.61E-03	761.02
NM_004235	KLF4	Kruppel-like factor 4 (gut)	0.96	6.64E-03	762.27
NM_172365	PPP1R36	Protein phosphatase 1, regulatory subunit 36	0.93	6.74E-03	765.82
NM_003665	FCN3	Ficolin (collagen/fibrinogen domain containing) 3 (Hakata antigen)	1.23	6.86E-03	770.05
NM_017910	TRMT61B	tRNA methyltransferase 61 homolog B (S. cerevisiae)	0.97	7.11E-03	778.71
NM_031459	SESN2	Sestrin 2	0.27	7.16E-03	780.18
NM_203458	NOTCH2NL	Notch 2 N-terminal like	0.59	7.16E-03	780.21
NM_002203	ITGA2	Integrin, α2 (CD49B, α2 subunit of VLA-2 receptor)	1.20	7.16E-03	780.44
NM_138337	CLEC12A	C-type lectin domain family 12, member A	1.32	7.22E-03	782.42
NM_020533	MCOLN1	Mucolipin 1	0.51	7.33E-03	786.12
NM_022481	ARAP3	ArfGAP with RhoGAP domain, ankyrin repeat and PH domain 3	1.11	7.42E-03	789.36
NM_001105578	SYCE2	Synaptonemal complex central element protein 2	1.13	7.66E-03	797.43
NM_021969	NR0B2	Nuclear receptor subfamily 0, group B, member 2	1.16	7.68E-03	798.17
NM_015852	ZNF117	Zinc finger protein 117	1.18	7.69E-03	798.86
NM_023946	LYNX1	Ly6/neurotoxin 1	1.10	7.89E-03	805.77
NM_001039887	PROSER3	Chromosome 19 open reading frame 55	1.17	7.94E-03	807.24
NM_015184	PLCL2	Phospholipase C-like 2	1.06	8.02E-03	809.76

Table II. Continued.

Gene reference	Gene symbol	Name	Mean	P-values (Up)	RP-values (Up)
NM_004938	DAPK1	Death-associated protein kinase 1	0.54	8.06E-03	811.54
NM_004755	RPS6KA5	Ribosomal protein S6 kinase, 90 kDa, polypeptide 5	1.04	8.21E-03	816.35
NM_001007532	STH	Saitohin	1.17	8.24E-03	817.51
NM_002613	PDPK1	3-Phosphoinositide-dependent protein kinase-1	1.10	8.34E-03	820.46
NM_006620	HBS1L	HBS1-like (S. cerevisiae)	1.04	8.46E-03	824.24
NM_003382	VIPR2	Vasoactive intestinal peptide receptor 2	0.77	8.55E-03	826.94
NM_203486	DLL3	δ-like 3 (*Drosophila*)	1.07	8.56E-03	827.15
NM_018010	IFT57	Intraflagellar transport 57 homolog (*Chlamydomonas*)	0.92	8.74E-03	833.66
NM_001135816	CXORF56	C1QTNF9B antisense RNA 1 (non-protein coding)	0.87	8.76E-03	834.30
NM_033133	CNP	2',3'-Cyclic nucleotide 3' phosphodiesterase	1.02	8.84E-03	836.32
NM_005199	CHRNG	Cholinergic receptor, nicotinic, γ	0.98	9.01E-03	841.20
NM_182765	HECTD2	HECT domain containing 2	0.79	9.12E-03	844.85
NM_001145290	SLC37A2	Solute carrier family 37 (glycerol-3-phosphate transporter), member 2	0.90	9.15E-03	845.70
NM_001195252	APTX	Aprataxin	1.05	9.31E-03	850.77
NM_001251964	TP53AIP1	Tumor protein p53-regulated apoptosis inducing protein 1	1.26	9.35E-03	851.82
NM_198270	NHS	Nance-Horan syndrome (congenital cataracts and dental anomalies)	1.13	9.53E-03	857.71
NM_000578	SLC11A1	Solute carrier family 11 (proton-coupled divalent metal ion transporters), member 1	1.06	9.63E-03	859.97
NM_002139	RBMX	RNA binding motif protein, X-linked	1.06	9.65E-03	860.47
NM_000435	NOTCH3	Notch 3	1.10	9.71E-03	862.14
NM_033066	MPP4	Membrane protein, palmitoylated 4 (MAGUK p55 subfamily member 4)	1.12	9.87E-03	867.43

B, Downregulated genes

Gene reference	Gene symbol	Name	Mean	P-values (Down)	RP-values (Down)
AJ298317	MUC5AC	Mucin 5AC, oligomeric mucus/ gel-forming	-2.54	8.43E-06	112.88
AF547222	LOC280665	Anti-CNG α1 cation channel translation product-like	-2.76	1.31E-05	123.92
AK097187	NQO2	NAD(P)H dehydrogenase, quinone 2	-2.48	3.75E-05	169.61
AK128551	RNF216	Ring finger protein 216	-2.19	6.09E-05	198.31
BC062748	EFCAB10	EF-hand calcium binding domain 10	-2.10	1.14E-04	233.55
NM_000639	FASLG	Fas ligand (TNF superfamily, member 6)	-1.61	2.15E-04	274.72
NM_001124	ADM	Adrenomedullin	-1.48	3.43E-04	311.18
NM_000043	FAS	Fas (TNF receptor superfamily, member 6)	-1.68	4.22E-04	329.27
BC065002	EXD3	Exonuclease 3'-5' domain containing 3	-2.04	5.19E-04	349.20
NM_004931	CD8B	CD8b molecule	-1.24	6.82E-04	378.73
NM_021635	PBOV1	Prostate and breast cancer overexpressed 1	-1.17	7.31E-04	386.63
NM_000093	COL5A1	Collagen, type V, α1	-1.67	8.08E-04	398.60
NM_000429	MAT1A	Methionine adenosyltransferase I, α	-1.67	8.43E-04	403.54

Table II. Continued.

Gene reference	Gene symbol	Name	Mean	P-values (Down)	RP-values (Down)
NM_000033	ABCD1	ATP-binding cassette, sub-family D (ALD), member 1	-1.69	8.92E-04	411.33
NM_000125	ESR1	Estrogen receptor 1	-1.67	8.95E-04	411.64
NM_000808	GABRA3	γ-Aminobutyric acid (GABA) A receptor, α3	-1.60	9.27E-04	415.96
NM_000595	LTA	Lymphotoxin-α (TNF superfamily, member 1)	-1.63	9.95E-04	427.69
NM_000197	HSD17B3	Hydroxysteroid (17-β) dehydrogenase 3	-1.67	1.04E-03	432.79
NM_001037442	RUFY3	RUN and FYVE domain containing 3	-1.54	1.05E-03	434.60
NM_000545	HNF1A	HNF1 homeobox A	-1.64	1.07E-03	437.31
NM_001005490	OR6C74	Olfactory receptor, family 6, subfamily C, member 74	-1.59	1.09E-03	439.40
NM_001031848	SERPINB8	Serpin peptidase inhibitor, clade B (ovalbumin), member 8	-1.54	1.15E-03	447.15
NM_000612	IGF2	Insulin-like growth factor 2 (somatomedin A)	-1.63	1.16E-03	448.01
NM_000517	HBA2	Hemoglobin, α2	-1.64	1.19E-03	451.63
NM_001130861	CLDN5	Claudin 5	-1.44	1.24E-03	458.33
NM_001004688	OR2M2	Olfactory receptor, family 2, subfamily M, member 2	-1.59	1.24E-03	458.57
NM_001030004	HNF4A	Hepatocyte nuclear factor 4, α	-1.56	1.26E-03	460.62
NM_001033952	CALCA	Calcitonin-related polypeptide α	-1.54	1.26E-03	461.21
NM_001010870	TDRD6	Tudor domain containing 6	-1.58	1.32E-03	466.23
NM_001018025	MTCP1	Mature T cell proliferation 1	-1.57	1.41E-03	475.20
NM_001012967	DDX60L	DEAD (Asp-Glu-Ala-Asp) box polypeptide 60-like	-1.57	1.41E-03	475.20
NM_001085	SERPINA3	Serpin peptidase inhibitor, clade A (α-1 antiproteinase, antitrypsin), member 3	-1.49	1.42E-03	476.63
NM_000633	BCL2	B-cell CLL/lymphoma 2	-1.63	1.45E-03	479.53
NM_001037666	GATSL3	GATS protein-like 3	-1.52	1.52E-03	486.52
NM_001165	BIRC3	Baculoviral IAP repeat containing 3	-1.42	1.58E-03	491.86
NM_002247	KCNMA1	Potassium large conductance calcium-activated channel, subfamily M, α member 1	-1.33	1.94E-03	521.16
NM_173625	C17ORF78	Chromosome 17 open reading frame 78	-1.01	1.95E-03	521.61
NM_001124759	FRG2C	FSHD region gene 2 family, member C	-1.44	2.00E-03	524.95
NM_001080453	INTS1	Integrator complex subunit 1	-1.51	2.00E-03	524.88
NM_004613	TGM2	Transglutaminase 2 (C polypeptide, protein-glutamine-γ-glutamyltransferase)	-1.24	2.14E-03	536.10
NM_001044392	MUC1	Mucin 1, cell surface-associated	-1.51	2.31E-03	548.26
NM_001195127	WI2-2373I1.2	Forkhead box L1-like	-1.39	2.41E-03	556.59
NM_001243042	HLA-C	Major histocompatibility complex, class I, C	-1.38	2.43E-03	558.50
NM_001083602	PTCH1	Patched 1	-1.49	2.58E-03	570.46
NM_207352	CYP4V2	Cytochrome P450, family 4, subfamily V, polypeptide 2	-0.86	2.71E-03	579.03
NR_029392	KRT16P2	Keratin 16 pseudogene 2	-0.54	2.97E-03	594.00
NM_001172646	PLCB4	Phospholipase C, β4	-1.39	3.03E-03	598.52
NM_002089	CXCL2	Chemokine (C-X-C motif) ligand 2	-1.34	3.39E-03	620.43
NM_001496	GFRA3	GDNF family receptor α3	-1.38	3.40E-03	620.75
NM_001668	ARNT	Aryl hydrocarbon receptor nuclear translocator	-1.37	3.42E-03	622.12
NM_021151	CROT	Carnitine O-octanoyltransferase	-1.18	3.47E-03	624.70

Table II. Continued.

Gene reference	Gene symbol	Name	Mean	P-values (Down)	RP-values (Down)
NM_001949	E2F3	E2F transcription factor 3	-1.36	3.53E-03	628.70
NM_002307	LGALS7	Lectin, galactoside-binding, soluble, 7	-1.32	3.56E-03	630.07
NM_001704	BAI3	Brain-specific angiogenesis inhibitor 3	-1.37	3.57E-03	630.78
NM_001978	DMTN	Erythrocyte membrane protein band 4.9 (dematin)	-1.35	3.62E-03	633.47
NM_183001	SHC1	SHC (Src homology 2 domain containing) transforming protein 1	-0.90	3.64E-03	634.32
NM_001185156	IL24	Interleukin 24	-1.39	3.71E-03	637.18
NM_004048	B2M	β-2-microglobulin	-1.27	3.73E-03	637.88
NM_001004456	OR1M1	Olfactory receptor, family 1, subfamily M, member 1	-1.60	3.85E-03	644.36
NM_002133	HMOX1	Heme oxygenase (decycling) 1	-1.33	3.97E-03	649.35
NM_002457	MUC2	Mucin 2, oligomeric mucus/gel-forming	-1.31	4.02E-03	651.72
NM_001198	PRDM1	PR domain containing 1, with ZNF domain	-1.39	4.05E-03	653.14
NM_001136022	NFATC4	Nuclear factor of activated T cells, cytoplasmic, calcineurin-dependent 4	-1.43	4.06E-03	653.68
NM_001454	FOXJ1	Horkhead box J1	-1.38	4.11E-03	656.34
NM_002006	FGF2	Fibroblast growth factor 2 (basic)	-1.35	4.11E-03	656.64
NM_177996	EPB41L1	Erythrocyte membrane protein band 4.1-like 1	-0.97	4.19E-03	659.94
NM_004417	DUSP1	Dual specificity phosphatase 1	-1.25	4.38E-03	669.42
NM_201282	EGFR	Epidermal growth factor receptor	-0.88	4.53E-03	676.59
NM_004416	DTX1	Deltex homolog 1 (*Drosophila*)	-1.25	4.68E-03	682.88
NM_003128	SPTBN1	Spectrin, β, non-erythrocytic 1	-1.29	4.75E-03	685.70
NM_001807	CEL	Carboxyl ester lipase (bile salt-stimulated lipase)	-1.36	4.94E-03	693.06
NM_207336	ZNF467	Zinc finger protein 467	-0.86	4.95E-03	693.44
NM_002381	MATN3	Matrilin 3	-1.32	5.00E-03	695.99
NM_002317	LOX	Lysyl oxidase	-1.32	5.00E-03	696.01
NM_024766	CAMKMT	Calmodulin-lysine N-methyltransferase	-1.15	5.07E-03	699.15
NM_003667	LGR5	Leucine-rich repeat containing G protein-coupled receptor 5	-1.29	5.27E-03	707.84
NM_002535	OAS2	2'-5'-Oligoadenylate synthetase 2, 69/71 kDa	-1.30	5.27E-03	708.15
NM_145041	TMEM106A	Transmembrane protein 106A	-1.10	5.27E-03	708.30
NM_003061	SLIT1	Slit homolog 1 (*Drosophila*)	-1.30	5.36E-03	711.28
NM_013292	MYLPF	Myosin light chain, phosphorylatable, fast skeletal muscle	-1.21	5.40E-03	712.71
NM_004310	RHOH	Ras homolog gene family, member H	-1.26	5.55E-03	719.34
NM_002483	CEACAM6	Carcinoembryonic antigen-related cell adhesion molecule 6	-1.30	5.71E-03	725.32
NM_005531	IFI16	Interferon, γ-inducible protein 16	-1.23	5.87E-03	732.01
NM_133471	PPP1R18	Protein phosphatase 1, regulatory subunit 18	-1.13	5.88E-03	732.45
NM_006398	UBD	Ubiquitin D	-1.22	5.89E-03	732.86
NM_004994	MMP9	Matrix metallopeptidase 9 (gelatinase B, 92 kDa gelatinase, 92 kDa type IV collagenase)	-1.24	5.90E-03	733.00
NR_003531	MEG3	Maternally expressed 3 (non-protein coding)	-0.79	5.98E-03	736.40
NM_012171	TSPAN17	Tetraspanin 17	-1.22	6.10E-03	741.06
NM_032599	FAM71F1	Family with sequence similarity 71, member F1	-1.14	6.13E-03	742.39
NM_019074	DLL4	δ-like 4 (*Drosophila*)	**-1.19**	**6.16E-03**	**743.53**
NM_002405	MFNG	MFNG O-fucosylpeptide 3-β-N-acetylglucosaminyltransferase	-1.31	6.30E-03	749.05
NM_015000	STK38L	Serine/threonine kinase 38-like	-1.21	6.32E-03	750.10
NM_018416	FOXJ2	Forkhead box J2	-1.20	6.36E-03	751.65
NM_016135	ETV7	Ets variant 7	-1.21	6.38E-03	752.29

Table II. Continued.

Gene reference	Gene symbol	Name	Mean	P-values (Down)	RP-values (Down)
NM_015886	PI15	Peptidase inhibitor 15	-1.21	6.39E-03	752.62
NM_002543	OLR1	Oxidized low density lipoprotein (lectin-like) receptor 1	-1.30	6.40E-03	752.88
NM_005023	PGGT1B	Protein geranylgeranyltransferase type I, β-subunit	-1.24	6.53E-03	757.78
NM_172390	NFATC1	Nuclear factor of activated T cells, cytoplasmic, calcineurin-dependent 1	-1.02	6.57E-03	759.52
NM_017766	CASZ1	Castor zinc finger 1	-1.20	6.78E-03	767.06
NM_144633	KCNH8	Potassium voltage-gated channel, subfamily H (eag-related), member 8	-1.12	6.86E-03	770.19
NM_025125	TMEM254	Chromosome 10 open reading frame 57	-1.14	6.87E-03	770.43
NM_182909	FILIP1L	Filamin A interacting protein 1-like	-0.92	6.89E-03	771.28
NM_173503	EFCAB3	EF-hand calcium binding domain 3	-1.02	6.92E-03	772.10
NM_144673	CMTM2	CKLF-like MARVEL transmembrane domain containing 2	-1.12	6.95E-03	773.54
NM_021819	LMAN1L	Lectin, mannose-binding, 1-like	-1.17	6.95E-03	773.62
NM_022804	SNURF	SNRPN upstream reading frame	-1.16	6.99E-03	775.02
NM_021633	KLHL12	Kelch-like 12 (*Drosophila*)	-1.17	7.01E-03	775.60
NM_021966	TCL1A	T cell leukemia/lymphoma 1A	-1.16	7.23E-03	782.50
NM_032637	SKP2	S phase kinase-associated protein 2 (p45)	-1.14	7.27E-03	784.16
NM_022648	TNS1	Tensin 1	-1.16	7.32E-03	785.88
NM_004213	SLC28A1	Solute carrier family 28 (sodium-coupled nucleoside transporter), member 1	-1.27	7.46E-03	790.45
NM_033088	STRIP1	Family with sequence similarity 40, member A	-1.14	7.49E-03	791.43
NM_022304	HRH2	Histamine receptor H2	-1.16	7.62E-03	796.01
NM_021105	PLSCR1	Phospholipid scramblase 1	-1.18	7.65E-03	797.28
NM_024768	EFCC1	Coiled-coil domain containing 48	-1.15	7.66E-03	797.48
NM_006290	TNFAIP3	Tumor necrosis factor, α-induced protein 3	-1.22	7.68E-03	798.22
NM_030639	BHLHB9	Basic helix-loop-helix domain containing, class B, 9	-1.14	7.69E-03	798.53
NM_004246	GLP2R	Glucagon-like peptide 2 receptor	-1.26	7.79E-03	802.00
NM_032873	UBASH3B	Ubiquitin-associated and SH3 domain containing B	-1.14	7.79E-03	802.14
NM_001963	EGF	Epidermal growth factor	-1.35	7.84E-03	803.92
NM_052904	KLHL32	Kelch-like 32 (*Drosophila*)	-1.13	7.89E-03	805.79
NM_006125	ARHGAP6	Rho GTPase activating protein 6	-1.23	7.90E-03	806.11
NM_032772	ZNF503	Zinc finger protein 503	-1.14	7.95E-03	807.90
NM_024886	C10orf95	Chromosome 10 open reading frame 95	-1.15	7.99E-03	809.09
NM_152703	SAMD9L	Sterile α motif domain containing 9-like	-1.09	8.02E-03	809.77
NM_032752	ZNF496	Zinc finger protein 496	-1.14	8.03E-03	810.31
NM_138456	BATF2	Basic leucine zipper transcription factor, ATF-like 2	-1.13	8.04E-03	810.45
NM_172370	DAOA	D-amino acid oxidase activator	-1.04	8.07E-03	811.67
NM_005747	CELA3A	Chymotrypsin-like elastase family, member 3A	-1.23	8.07E-03	811.75
NM_033101	LGALS12	Lectin, galactoside-binding, soluble, 12	-1.14	8.14E-03	813.87
NM_012224	NEK1	NIMA (never in mitosis gene a)-related kinase 1	-1.21	8.21E-03	816.40
NM_020436	SALL4	Sal-like 4 (*Drosophila*)	-1.19	8.31E-03	819.74
NM_138980	MAPK10	Mitogen-activated protein kinase 10	-1.13	8.34E-03	820.62
NM_020896	OSBPL5	Oxysterol binding protein-like 5	-1.18	8.41E-03	822.84

Table II. Continued.

Gene reference	Gene symbol	Name	Mean	P-values (Down)	RP-values (Down)
NM_052897	MBD6	Methyl-CpG binding domain protein 6	-1.14	8.52E-03	826.04
NM_207419	C1QTNF8	C1q and tumor necrosis factor related protein 8	-0.82	8.58E-03	827.94
NM_005933	KMT2A	myeloid/lymphoid or mixed-lineage leukemia (trithorax homolog, *Drosophila*)	-1.23	8.59E-03	828.40
NM_181712	KANK4	KN motif and ankyrin repeat domains 4	-0.96	8.61E-03	828.96
NM_017777	MKS1	Meckel syndrome, type 1	-1.20	8.61E-03	829.20
NM_176677	NHLRC4	NHL repeat containing 4	-0.99	8.67E-03	831.05
NM_025130	HKDC1	Hexokinase domain containing 1	-1.14	8.71E-03	832.53
NM_017654	SAMD9	Sterile α motif domain containing 9	-1.21	8.92E-03	838.42
NM_052864	TIFA	TRAF-interacting protein with forkhead-associated domain	-1.14	8.94E-03	838.99
NM_015569	DNM3	Dynamin 3	-1.21	8.95E-03	839.17
NM_139047		Mitogen-activated protein kinase 8	-1.12	8.99E-03	840.70
NM_207173	NPSR1	Neuropeptide S receptor 1	-0.87	9.03E-03	841.91
NM_015444	TMEM158	Transmembrane protein 158 (gene/pseudogene)	-1.21	9.03E-03	841.90
NM_017523	XAF1	XIAP-associated factor 1	-1.21	9.10E-03	844.23
NM_006931	SLC2A3	Solute carrier family 2 (facilitated glucose transporter), member 3	-1.22	9.11E-03	844.45
NM_019018	FAM105A	Family with sequence similarity 105, member A	-1.19	9.13E-03	845.15
NM_153042	KDM1B	Lysine (K)-specific demethylase 1B	-1.08	9.18E-03	846.40
NM_033056	PCDH15	Protocadherin-related 15	-1.14	9.23E-03	848.31
NM_014157	CCDC113	Coiled-coil domain containing 113	-1.21	9.25E-03	848.53
NM_144962	PEBP4	Phosphatidylethanolamine-binding protein 4	-1.12	9.31E-03	850.61
NM_145862	CHEK2	Checkpoint kinase 2	-1.09	9.36E-03	852.29
NM_182524	ZNF595	Zinc finger protein 595	-0.93	9.41E-03	853.59
NM_014858	TMCC2	Transmembrane and coiled-coil domain family 2	-1.21	9.46E-03	855.35
NM_144990	SLFNL1	Schlafen-like 1	-1.11	9.47E-03	855.60
NM_022147	RTP4	Receptor (chemosensory) transporter protein 4	-1.16	9.49E-03	856.25
NM_022873	IFI6	Interferon, α-inducible protein 6	-1.16	9.73E-03	863.03
NM_152685	SLC23A1	Solute carrier family 23 (nucleobase transporters), member 1	-1.09	9.73E-03	863.10
NM_152278	TCEAL7	Transcription elongation factor A (SII)-like 7	-1.09	9.84E-03	866.45
NM_019035	PCDH18	Protocadherin 18	-1.19	9.95E-03	869.75
NM_153183	NUDT10	Nudix (nucleoside diphosphate linked moiety X)-type motif 10	-1.07	9.99E-03	870.83

Fig. 3A, treatment with this agent dose-dependently induced differentiation as assessed by ALP activity. Concordantly, this agent also induced *MT1G* and *MT2A* mRNA levels, in close correlation to ALP activity (Pearson r=0.993, p=0.007 for *MT1G* and r=0.999, p=0.0006 for *MT2A*; Fig. 3B). To determine whether the induction of MTs has a functional role in butyrate-induced differentiation, we used siRNAs to inhibit the induction of only *MT1G* (si1G.1 and si1G.2) or of all MT1 and MT2 isoforms (siMTs), as previously described (12). Fig. 3C shows that siRNA pre-treatment partially mitigated *MT1G* induction after BUT treatment and markedly, also diminished the induction of *CDX2* (Fig. 3D), and of goblet-cell marker *TFF3* (Fig. 3E). Notably, BUT treatment had no effect on mRNA levels of *MUC2*, as has been previously reported by others (17) (data not shown). In contrast, although the enterocyte-specific markers *HSI* and *CA1* were markedly upregulated at 2 mM BUT, silencing of MTs had no effect on their induction (Fig. 3F and G), or on the cell-cycle arrest mediator *CDKN1A/p21* (data not shown), whereas ALP activity was only slightly, but significantly reduced (Fig. 3H).

We next treated HT-29 MOCK and MT1G$^+$ cells with butyrate. Notably, as depicted in Fig. 4A, whereas *CDX2*

Table III. Significant functional categories of upregulated and downregulated genes.

A, Upregulated genes	P-value	Bonferroni	Benjamini	FDR
GO category				
Cell fate commitment	7.2E-07	8.9E-04	8.9E-04	1.2E-03
Negative regulation of cell differentiation	2.9E-05	3.5E-02	1.2E-02	4.7E-02
Differentiation	6.8E-05	1.7E-02	1.7E-02	8.8E-02
Developmental protein	9.2E-05	2.4E-02	1.2E-02	1.2E-01
Notch signaling pathway	1.0E-04	2.6E-02	8.7E-03	1.3E-01
Intestine	2.4E-04	6.0E-02	1.5E-02	3.1E-01
KEGG pathway				
Notch signaling pathway	3.5E-05	2.7E-03	2.7E-03	3.7E-02
B, Downregulated genes				
GO category				
Regulation of cell death	5.9E-07	9.2E-04	4.6E-04	9.8E-04
Regulation of cell proliferation	1.8E-04	2.4E-01	1.9E-02	2.9E-01
Regulation of cell migration	2.0E-04	2.7E-01	1.9E-02	3.3E-01
KEGG pathway				
Pathways in cancer	1.9E-04	1.6E-02	1.6E-02	2.1E-01

GO, Gene Ontology; KEGG, Kyoto Encyclopedia of Genes and Genomes; FDR, false discovery rate.

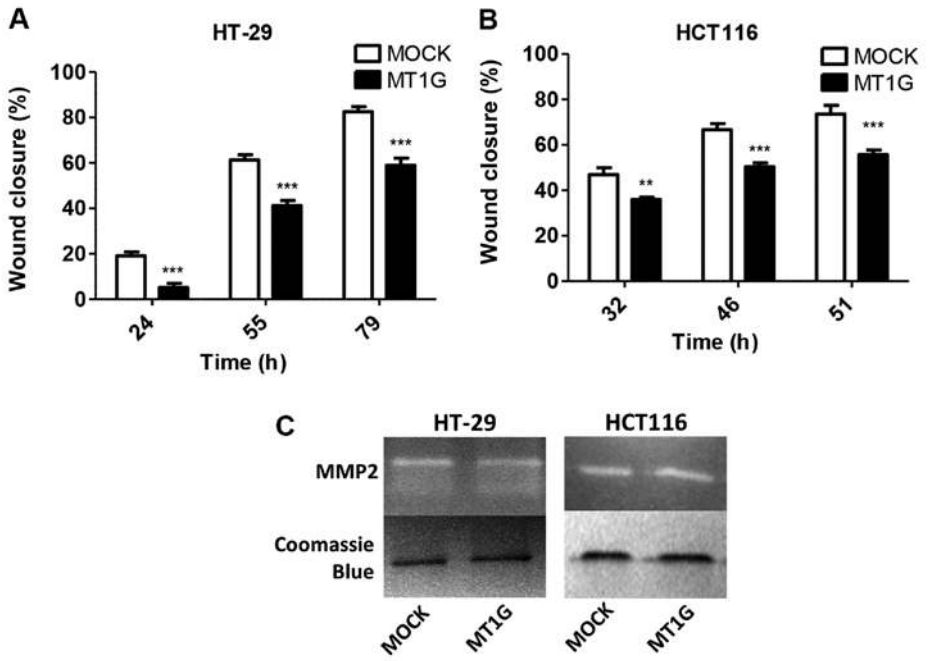

Figure 2. Wound healing 'scratch' assays in (A) HT-29 and (B) HCT116 MT1G^{+} cells showing decreased migration capacity, but no difference in MMP2 activity as measured by (C) gelatin zymography; $^{*}p<0.05$, $^{**}p<0.01$ and $^{***}p<0.001$.

mRNA levels were similarly induced, MT1G overexpression markedly enhanced the induction of *TFF3* (Fig. 4B), whereas it blunted that of *HSI* (Fig. 4C). Therefore, both silencing and overexpression of MT1G support the hypothesis that this gene favors goblet over enterocyte differentiation upon butyrate treatment of HT-29 cells.

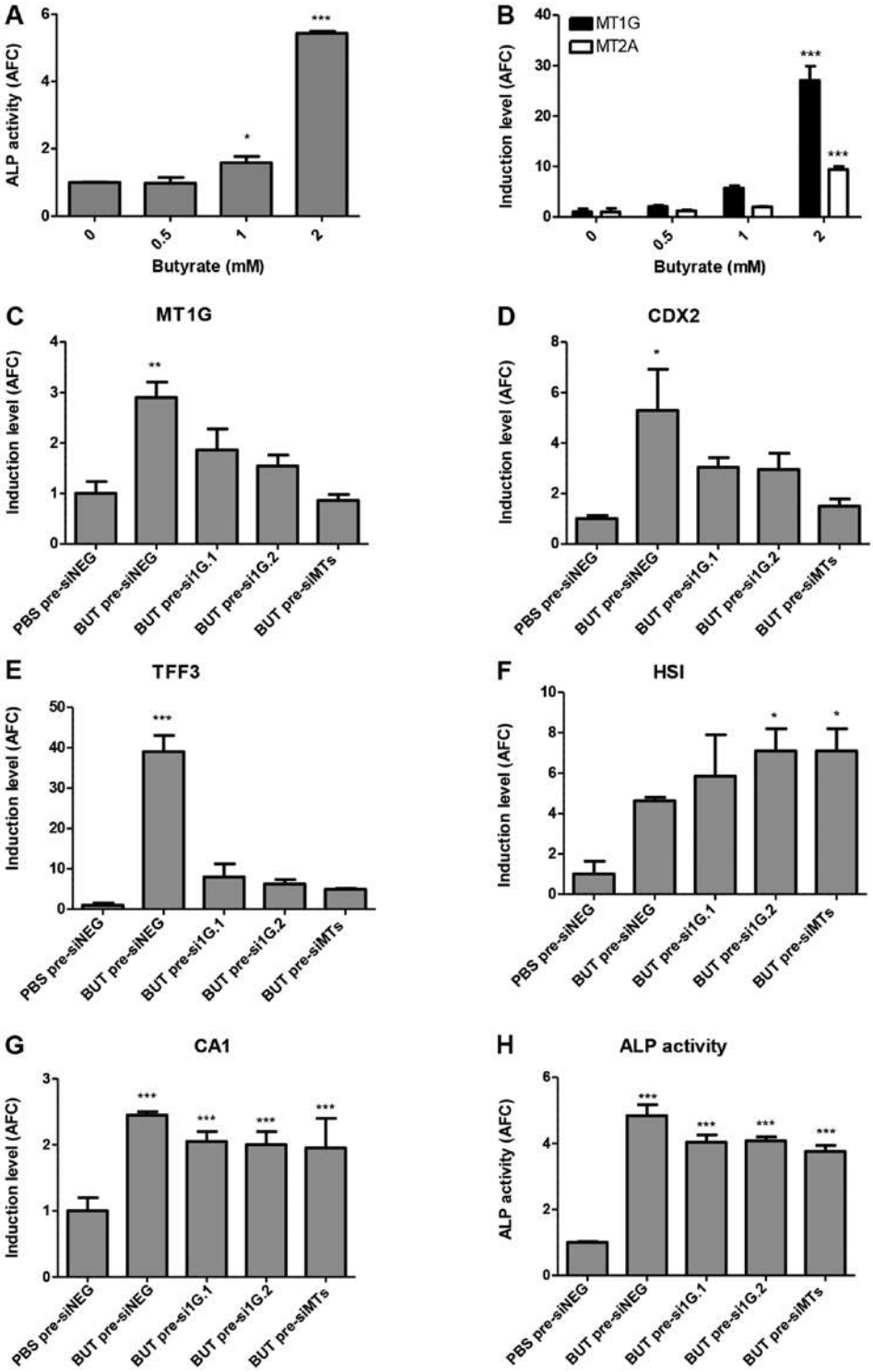

Figure 3. Butyrate mediates the differentiation of HT-29 cells. (A) Assessment of ALP enzymatic activity, 72 h after treatment. (B) Induction of MT1G and MT2A mRNA expression measured by qRT-PCR 72 h after treatment. (C-G) Expression of MT1G, CDX2, TFF3, HSI and CA1 as well as (H) ALP activity after siRNA-mediated silencing of MT1G or all MTs. AFC, average fold-change; $^{*}p<0.05$, $^{**}p<0.01$ and $^{***}p<0.001$.

Involvement of MT1G in post-confluent differentiation of HT-29 cells. Next, we studied the expression of MT1G in the post-confluent growth of HT-29 cells, where this cell line is known to differentiate poorly (20). In this setting, *MT1G* mRNA was transiently induced at day 1 post-confluence, after which its expression was significantly reduced (Fig. 5A). In contrast, *CDX2* and enterocyte-specific genes *HSI* and *CA1* were transiently induced at day 3, two days after *MT1G* induction (Fig. 5B-D). Notably, *TFF3* expression mirrors *MT1G* expression, until day 14 when it is induced again (Fig. 5E). These time-course analyses again favored the association of MT1G induction with goblet over enterocyte differentiation. Notably, as with BUT treatment, *MUC2* expression was not altered in this context (Fig. 5F). We were unable to perform

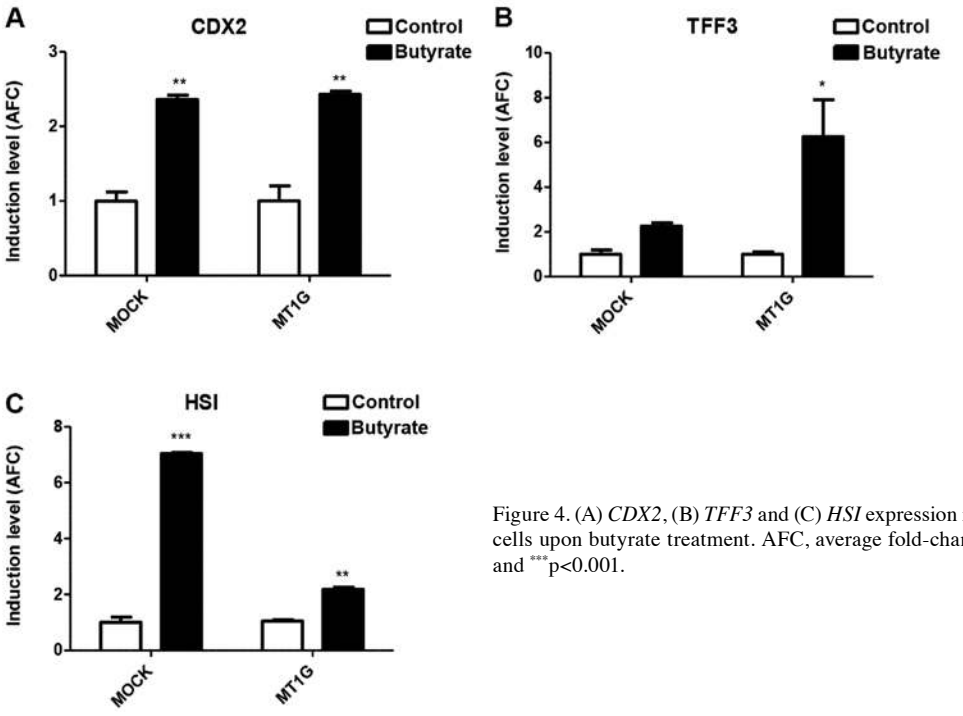

Figure 4. (A) *CDX2*, (B) *TFF3* and (C) *HSI* expression in MOCK and MT1G^{+} cells upon butyrate treatment. AFC, average fold-change; *p<0.05, **p<0.01 and ***p<0.001.

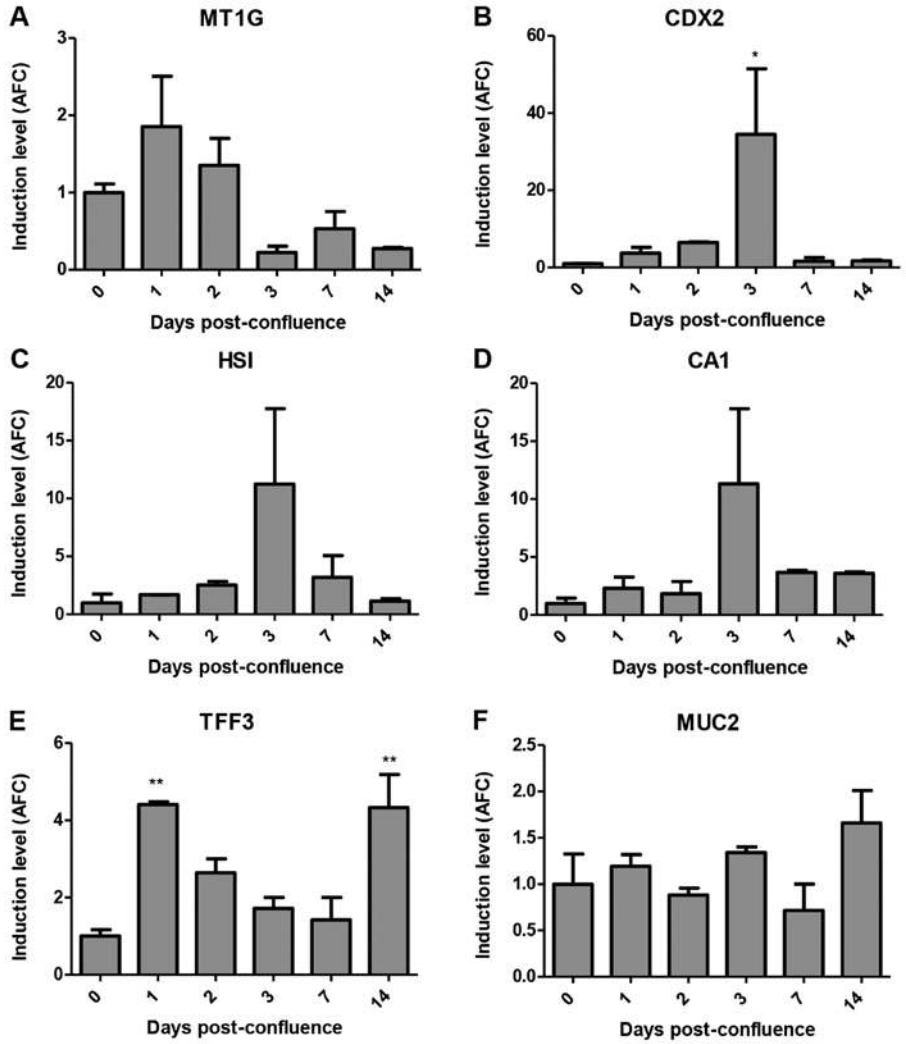

Figure 5. Expression of (A) *MT1G*, (B) *CDX2*, (C) *HIS*, (D) *CA1*, (E) *TFF3* and (F) *MUC2* upon differentiation stimulated by post-confluent growth of HT-29 cells. AFC, average fold-change; *p<0.05, **p<0.01 and ***p<0.001.

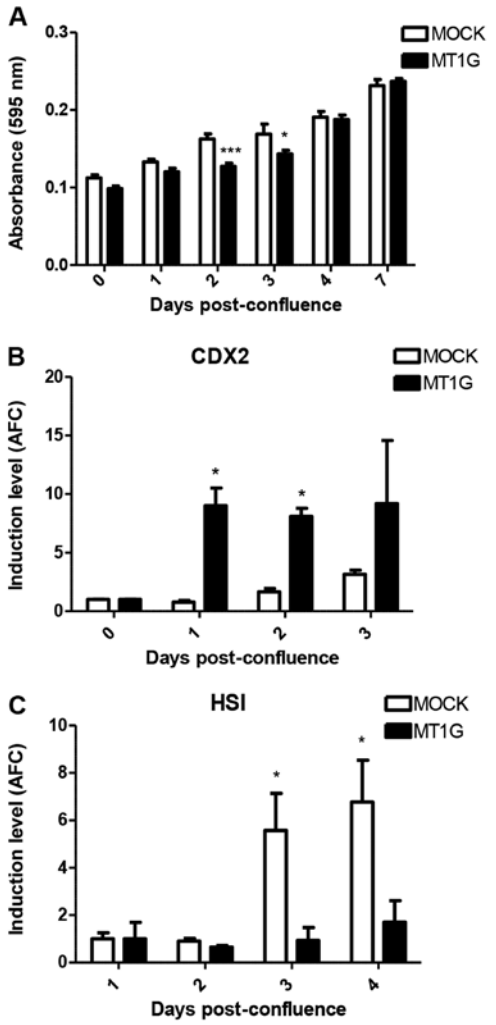

Figure 6. Effects of stable MT1G expression on post-confluent growth of HT-29 cells. (A) ALP activity. (B) *CDX2* and (C) *HSI* expression. AFC, average fold-change; $^{*}p<0.05$, $^{**}p<0.01$ and $^{***}p<0.001$.

siRNA-mediated silencing of MT1G in this setting, as cells did not survive in a totally confluent state for >1 day after transfection.

When growing HT-29 MOCK and MT1G^{+} cells post-confluence, we noted no difference in the induction of ALP activity between these two cell lines (Fig. 6A). Notably however, in the latter, *CDX2* mRNA was induced at significantly higher levels (Fig. 6B) whereas *HSI* induction was abolished (Fig. 6C). While we noted no differences in the induction of *TFF3* mRNA (data not shown), our data also implies a role for MT1G expression in counteracting enterocyte differentiation of HT-29 cells.

Labile zinc levels in butyrate-treated and post-confluent HT-29 cells. Given the close relationship between MTs and zinc biology, we analyzed the levels of intracellular labile zinc in both models of differentiation, using the zinc-specific fluorophore FZ. Notably, after 72 h of 2 mM BUT treatment, FZ intensity was significantly induced in the HT-29 cells (Fig. 7A). We used TPEN treatment to chelate intracellular labile zinc before the addition of butyrate, and found that this abolished both *CDX2* and *HSI* mRNA induction (Fig. 7B and C), but had no effect on *TFF3* levels (Fig. 7D). In the post-confluence model, as shown by fluorescence microscopy in Fig. 7E and by fluorimetry in Fig. 7F, FZ intensity was induced at day 2 and progressively increased thereafter. Given that TPEN exposure for >6 h is toxic to HT-29 cells, we used daily 5-h TPEN treatments to evaluate the effect of labile zinc on goblet and enterocyte markers. Notably, *TFF3* mRNA expression was significantly induced at days 1-3 post-confluence in TPEN-treated cells (Fig. 7G), whereas there was no effect on either *CDX2* or *HSI* levels (not shown).

In summary, labile zinc was induced in both models of intestinal differentiation, and its chelation by TPEN treatment either inhibited enterocyte differentiation (butyrate model) or induced the expression of goblet-cell markers (post-confluency model).

Discussion

In the present study, we uncovered a new role for MT1G in altering the differentiation properties of the HT-29 cell line. We previously showed that induction of MTs by HDACi agents such as trichostatin A and sodium butyrate (BUT) is at least partly responsible for their cytostatic effects on human CRC cell lines, and that exogenous MT1G overexpression in the colorectal HCT116 cell line resulted in growth inhibition in nude mouse xenografts (12). Notably, whereas MT1G overexpression did not alter the *in vivo* xenograft growth rate of HT-29 cells, it markedly increased the number of goblet cells and differentiation markers of these tumors, both of the goblet and the enterocyte lineages. These effects were not readily observed in 2D culture (data not shown), suggesting that additional signals from the tumor microenvironment may be needed to fulfill this effect. The reasons for the different observed phenotypic consequences of MT1G overexpression in these two cell lines are unclear, but a possible explanation may stem from the differences in endogenous MT1G expression: HCT116 cells do not express MT1G due to promoter hypermethylation and therefore the impact of MT1G overexpression may be stronger than that in HT-29 cells, which express low, but detectable mRNA levels (8).

In an effort to understand the molecular mechanisms underlying the altered differentiation of MT1G^{+} tumors, we performed mRNA expression profiling by cDNA microarrays. The expression of several genes involved in the regulation of cell differentiation was found to be altered, particularly in the Notch signaling pathway, whose inhibition is well known to stimulate goblet cell differentiation in the intestine through activation of ATOH1 (22). Notably, markers of different sets of intestinal stem cell markers were differentially dysregulated in MT1G^{+} tumors, with upregulation of HOPX (expressed in quiescent stem cells) and downregulation of Lgr5 (in crypt base columnar stem cells), again suggesting altered differentiation hierarchies (23,24). Further studies are warranted to explore this in further detail.

To further characterize the involvement of MT1G in colorectal differentiation, we relied on two well-studied cell culture conditions: sodium butyrate and post-confluent growth. We showed that endogenous MT1G induction was required for the induction of goblet cell markers by butyrate, and was temporally associated with such markers in the confluency

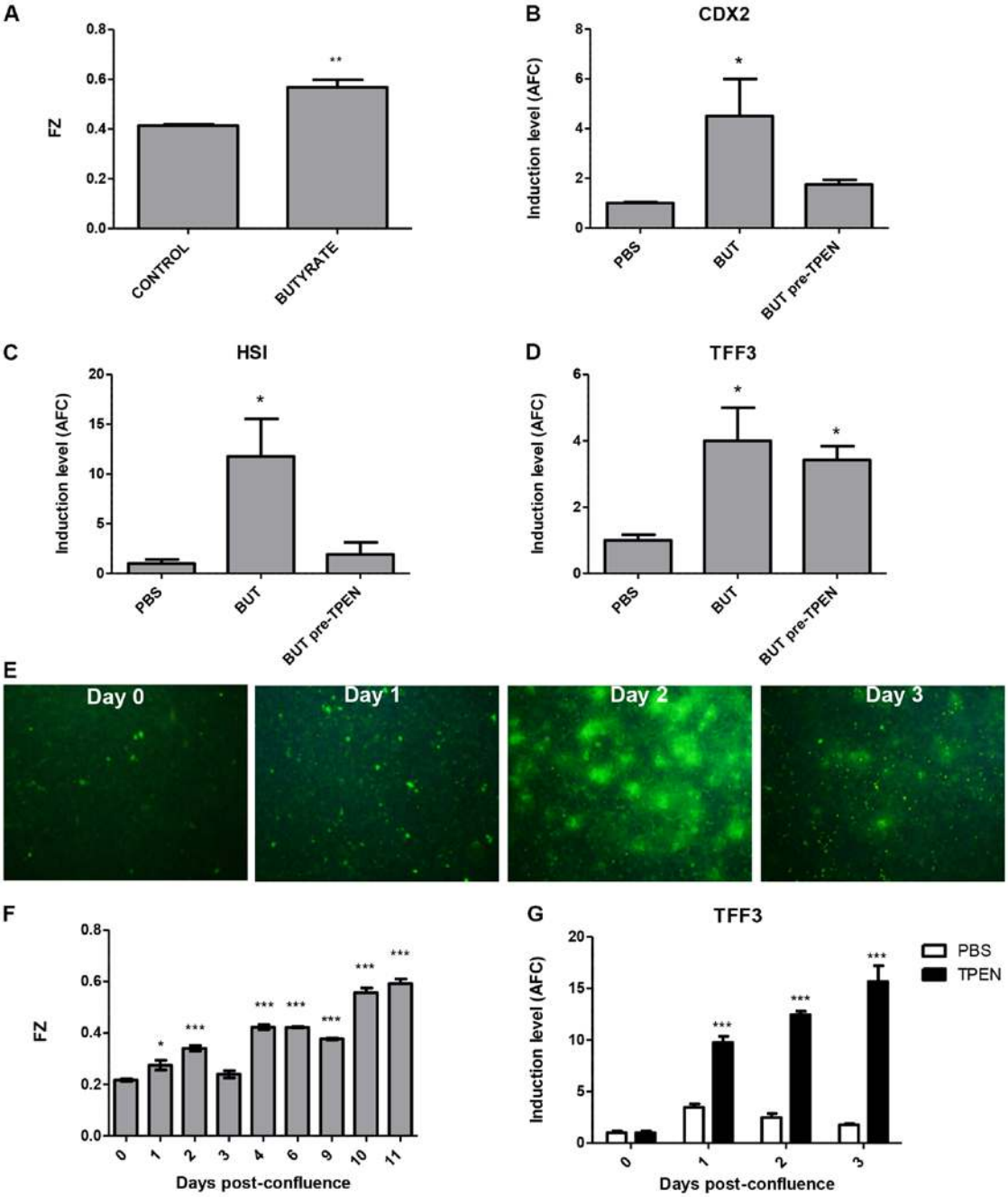

Figure 7. Labile zinc induction upon differentiation. (A) Butyrate induces intracellular labile zinc levels in HT-29 cells, as measured by fluorimetry using the Fluozin-3AM (FZ) probe. (B and C) Both *CDX2* and *HSI* induction by butyrate are blunted by TPEN pre-treatment, whereas there is no effect on (D) *TFF3* expression. (E and F) Labile zinc levels are also increased in the post-confluency differentiation model of HT-29 cells, as measured by (E) epifluorescence microscopy (F) and fluorimetry. (G) Daily doses of TPEN stimulate TFF3 expression of post-confluent cultures. AFC, average fold-change; $^{*}p<0.05$, $^{**}p<0.01$ and $^{***}p<0.001$.

model. Moreover, stable exogenous MT1G overexpression favored goblet and blunted enterocyte differentiation in both models. Previous studies have shown MTs to be upregulated *in vitro* upon CRC differentiation (25), and demonstrated a role for MTs in modulating differentiation in different tissues, such as human salivary gland tumor cells (where MT1F overexpression resulted in slower growing and more differentiated tumors) (26), leukemic (27) neurons and glial (28), and T cells (29). However, to the best of our knowledge, this is the first study showing a direct functional involvement of a metallothionein isoform in CRC differentiation.

Labile zinc ions have been recognized as secondary messengers capable of transducing a wide variety of intracellular signals (30,31), including differentiation (32-34). MTs can regulate labile zinc concentrations and zinc transfer to different cellular organelles (35), as well as respond to changes in intracellular zinc ions (36). We showed in the present study that labile zinc was increased during differentiation induced both by butyrate and confluency, and that this was required for enterocyte differentiation by butyrate, whereas it blunted goblet marker induction in post-confluency. While the reason behind the differences observed in both models are unclear,

the overall effects of zinc induction favor an enterocyte over goblet differentiation. Notably, although labile zinc increases have already been reported to occur during butyrate-mediated differentiation of the HT-29 cell line and have been associated to defined stages of the cell cycle (37), in the present study, we reported for the first time a functional consequence of labile zinc induction in this process. Previous studies in other tissues have shown that MTs transiently translocate to the nucleus during early phases of differentiation to release the zinc ions necessary for zinc-dependent transcription factors to execute the differentiation programs of adipocytes and myoblasts (38,39). Although we previously showed that MTs in HT-29 are localized to the cytoplasm (8), we were not able to detect a nuclear shift in either of the differentiation models that we used in the present study (data not shown), although this possibility should be studied in further detail.

Taking into account our results, we hypothesize that MT1G induction during differentiation may play a role in the chelation and re-distribution of intracellular labile zinc, perhaps modulating the activity of zinc-requiring transcription factors and enzymes, and stimulating the differentiation program of colorectal cells. *In vitro*, our results showed that MT1G favors a goblet over enterocyte differentiation, although our mouse xenografts assays suggest that *in vivo* the differentiation into enterocytes is also stimulated, perhaps as a compensatory mechanism or in a non-cell autonomous manner. The precise mechanisms whereby this occurs and the participation of MT1G (and other MTs) in labile zinc redistribution during differentiation need to be studied in further detail. Moreover, tumor classifications based on gene signatures associated with different cell types suggest that tumors of the more differentiated 'goblet-' or 'enterocyte-like' subtypes have a better prognosis than undifferentiated 'stem-like' subtype, as well as different responses to therapeutic agents. Therefore, better understanding of the molecular mechanisms that govern the differentiation processes of tumor cells may be of clinical relevance.

Overall, in the present study, we unveiled a pro-differentiation effect of MT1G on various CRC cells, thus proposing a new mechanism whereby MT1G may act as a tumor suppressor in this tumor type. Moreover, we established a functional consequence of transient increases in labile zinc upon differentiation stimuli, and support the need of further studies relating zinc signaling and differentiation, that may ultimately underlie tumor cell phenotypes and response to therapies.

Acknowledgements

The present study was funded by the Consejo Nacional de Investigaciones Científicas y Técnicas (CONICET) (PIP no. 845-10 to M.B.), the Agencia Nacional de Promoción Científica y Tecnológica (ANPCyT) (IP-PAE 2007, to J.M.), the Fundación Cáncer, the Fundación P. Mosoteguy, the Fundación Sales, and the Fundación María Calderón de la Barca, Buenos Aires, Argentina.

References

1. Torre LA, Bray F, Siegel RL, Ferlay J, Lortet-Tieulent J and Jemal A: Global cancer statistics, 2012. CA Cancer J Clin 65: 87-108, 2015.
2. Dalerba P, Kalisky T, Sahoo D, Rajendran PS, Rothenberg ME, Leyrat AA, Sim S, Okamoto J, Johnston DM, Qian D, *et al*: Single-cell dissection of transcriptional heterogeneity in human colon tumors. Nat Biotechnol 29: 1120-1127, 2011.
3. Sadanandam A, Lyssiotis CA, Homicsko K, Collisson EA, Gibb WJ, Wullschleger S, Ostos LC, Lannon WA, Grotzinger C, Del Rio M, *et al*: A colorectal cancer classification system that associates cellular phenotype and responses to therapy. Nat Med 19: 619-625, 2013.
4. Pedersen MO, Larsen A, Stoltenberg M and Penkowa M: The role of metallothionein in oncogenesis and cancer prognosis. Prog Histochem Cytochem 44: 29-64, 2009.
5. Eckschlager T, Adam V, Hrabeta J, Figova K and Kizek R: Metallothioneins and cancer. Curr Protein Pept Sci 10: 360-375, 2009.
6. Dziegiel P, Pula B, Kobierzycki C, Stasiolek M and Podhorska-Okolow M: Metallothioneins in normal and cancer cells. Adv Anat Embryol Cell Biol 218: 1-117, 2016.
7. Gumulec J, Raudenska M, Adam V, Kizek R and Masarik M: Metallothionein - immunohistochemical cancer biomarker: A meta-analysis. PLoS One 9: e85346, 2014.
8. Arriaga JM, Levy EM, Bravo AI, Bayo SM, Amat M, Aris M, Hannois A, Bruno L, Roberti MP, Loria FS, *et al*: Metallothionein expression in colorectal cancer: Relevance of different isoforms for tumor progression and patient survival. Hum Pathol 43: 197-208, 2012.
9. Arriaga JM, Bravo IA, Bruno L, Morales Bayo S, Hannois A, Sanchez Loria F, Pairola F, Huertas E, Roberti MP, Rocca YS, *et al*: Combined metallothioneins and p53 proteins expression as a prognostic marker in patients with Dukes stage B and C colorectal cancer. Hum Pathol 43: 1695-1703, 2012.
10. Janssen AM, van Duijn W, Oostendorp-Van De Ruit MM, Kruidenier L, Bosman CB, Griffioen G, Lamers CB, van Krieken JH, van De Velde CJ and Verspaget HW: Metallothionein in human gastrointestinal cancer. J Pathol 192: 293-300, 2000.
11. Bianchini M, Levy E, Zucchini C, Pinski V, Macagno C, De Sanctis P, Valvassori L, Carinci P and Mordoh J: Comparative study of gene expression by cDNA microarray in human colorectal cancer tissues and normal mucosa. Int J Oncol 29: 83-94, 2006.
12. Arriaga JM, Greco A, Mordoh J and Bianchini M: Metallothionein 1G and zinc sensitize human colorectal cancer cells to chemotherapy. Mol Cancer Ther 13: 1369-1381, 2014.
13. Cleveland WS, Devlin SJ and Grosse E: Regression by local fitting: Methods, properties, and computational algorithm. J Econom 37: 87-114, 1988.
14. Yang YH, Dudoit S, Luu P, Lin DM, Peng V, Ngai J and Speed TP: Normalization for cDNA microarray data: A robust composite method addressing single and multiple slide systematic variation. Nucleic Acids Res 30: e15, 2002.
15. Dennis G Jr, Sherman BT, Hosack DA, Yang J, Gao W, Lane HC and Lempicki RA: DAVID: Database for Annotation, Visualization, and Integrated Discovery. Genome Biol 4: 3, 2003.
16. Huang W, Sherman BT and Lempicki RA: Systematic and integrative analysis of large gene lists using DAVID bioinformatics resources. Nat Protoc 4: 44-57, 2009.
17. Velcich A, Palumbo L, Jarry A, Laboisse C, Racevskis J and Augenlicht L: Patterns of expression of lineage-specific markers during the in vitro-induced differentiation of HT29 colon carcinoma cells. Cell Growth Differ 6: 749-757, 1995.
18. Troeberg L and Nagase H: Zymography of metalloproteinases. Curr Protoc Protein Sci 21: Unit 21.15, 2004.
19. Augeron C and Laboisse CL: Emergence of permanently differentiated cell clones in a human colonic cancer cell line in culture after treatment with sodium butyrate. Cancer Res 44: 3961-3969, 1984.
20. Zweibaum A, Pinto M, Chevalier G, Dussaulx E, Triadou N, Lacroix B, Haffen K, Brun JL and Rousset M: Enterocytic differentiation of a subpopulation of the human colon tumor cell line HT-29 selected for growth in sugar-free medium and its inhibition by glucose. J Cell Physiol 122: 21-29, 1985.
21. Chung YS, Song IS, Erickson RH, Sleisenger MH and Kim YS: Effect of growth and sodium butyrate on brush border membrane-associated hydrolases in human colorectal cancer cell lines. Cancer Res 45: 2976-2982, 1985.
22. VanDussen KL, Carulli AJ, Keeley TM, Patel SR, Puthoff BJ, Magness ST, Tran IT, Maillard I, Siebel C, Kolterud Å, *et al*: Notch signaling modulates proliferation and differentiation of intestinal crypt base columnar stem cells. Development 139: 488-497, 2012.

23. Barker N, Ridgway RA, van Es JH, van de Wetering M, Begthel H, van den Born M, Danenberg E, Clarke AR, Sansom OJ and Clevers H: Crypt stem cells as the cells-of-origin of intestinal cancer. Nature 457: 608-611, 2009.
24. Takeda N, Jain R, LeBoeuf MR, Wang Q, Lu MM and Epstein JA: Interconversion between intestinal stem cell populations in distinct niches. Science 334: 1420-1424, 2011.
25. Vecchini F, Pringault E, Billiar TR, Geller DA, Hausel P and Felley-Bosco E: Decreased activity of inducible nitric oxide synthase type 2 and modulation of the expression of glutathione *S*-transferase α, bcl-2, and metallothioneins during the differentiation of CaCo-2 cells. Cell Growth Differ 8: 261-268, 1997.
26. Hecht D, Jung D, Prabhu VV, Munson PJ, Hoffman MP and Kleinman HK: Metallothionein promotes laminin-1-induced acinar differentiation in vitro and reduces tumor growth in vivo. Cancer Res 62: 5370-5374, 2002.
27. Maghdooni Bagheri P, Govaerts I and De Ley M: Role of metallothionein in differentiation of leukemia cells. Mol Biol Rep 38: 3017-3022, 2011.
28. Nishikawa M, Mori H and Hara M: Reduced zinc cytotoxicity following differentiation of neural stem/progenitor cells into neurons and glial cells is associated with upregulation of metallothioneins. Environ Toxicol Pharmacol 39: 1170-1176, 2015.
29. Wu C, Pot C, Apetoh L, Thalhamer T, Zhu B, Murugaiyan G, Xiao S, Lee Y, Rangachari M, Yosef N, *et al*: Metallothioneins negatively regulate IL-27-induced type 1 regulatory T cell differentiation. Proc Natl Acad Sci USA 110: 7802-7807, 2013.
30. Murakami M and Hirano T: Intracellular zinc homeostasis and zinc signaling. Cancer Sci 99: 1515-1522, 2008.
31. Yamasaki S, Sakata-Sogawa K, Hasegawa A, Suzuki T, Kabu K, Sato E, Kurosaki T, Yamashita S, Tokunaga M, Nishida K, *et al*: Zinc is a novel intracellular second messenger. J Cell Biol 177: 637-645, 2007.
32. Beyersmann D and Haase H: Functions of zinc in signaling, proliferation and differentiation of mammalian cells. Biometals 14: 331-341, 2001.
33. Dubben S, Hönscheid A, Winkler K, Rink L and Haase H: Cellular zinc homeostasis is a regulator in monocyte differentiation of HL-60 cells by 1 alpha,25-dihydroxyvitamin D3. J Leukoc Biol 87: 833-844, 2010.
34. Wolford JL, Chishti Y, Jin Q, Ward J, Chen L, Vogt S and Finney L: Loss of pluripotency in human embryonic stem cells directly correlates with an increase in nuclear zinc. PLoS One 5: e12308, 2010.
35. Maret W: Metals on the move: Zinc ions in cellular regulation and in the coordination dynamics of zinc proteins. Biometals 24: 411-418, 2011.
36. Kindermann B, Döring F, Pfaffl M and Daniel H: Identification of genes responsive to intracellular zinc depletion in the human colon adenocarcinoma cell line HT-29. J Nutr 134: 57-62, 2004.
37. Krezel A and Maret W: Zinc-buffering capacity of a eukaryotic cell at physiological pZn. J Biol Inorg Chem 11: 1049-1062, 2006.
38. Schmidt C and Beyersmann D: Transient peaks in zinc and metallothionein levels during differentiation of 3T3L1 cells. Arch Biochem Biophys 364: 91-98, 1999.
39. Apostolova MD, Ivanova IA and Cherian MG: Metallothionein and apoptosis during differentiation of myoblasts to myotubes: Protection against free radical toxicity. Toxicol Appl Pharmacol 159: 175-184, 1999.